encit 2020

ABCM Associação Brasileira de Engenharia e Ciências Mecânicas

18th Brazilian Congress of Thermal Sciences and Engineering
November 16-20, 2020 (Online)

ENC-2020-0640
ASSESSMENT OF THE ELLIPTIC BLENDING RSM TURBULENCE MODEL ON A WIND TURBINE-TYPE ROTOR UNDER MILDLY COMPRESSIBLE BLADE TIP FLOW REGIME

Marco Leonardelli Lovatto
Adriane Prisco Petry
PROMEC - Universidade Federal do Rio Grande do Sul – R. Sarmento Leite, 425 – Porto Alegre, Brazil.
marco.lovatto@ufrgs.br; marcolovatto@gmail.com; adrianep@mecanica.ufrgs.br

Abstract. *Large multi-megawatt horizontal axis wind turbines (HAWTs) may encounter mildly compressible flow regimes at the suction side of the blade tip, a phenomenon that should be assessed with caution by using CFD strategies capable of capturing it, especially if blade tip vortices, aeroelasticity and aeroacoustics are of interest. This work aims to stimulate the development of such strategies as high-fidelity references for the improvement of low-fidelity (engineering) models, such as Blade Element Momentum (BEM) and Vortex Wake Models (VWM). Differently from two-equation turbulence models, which generally rely on the assumption of isotropic turbulence, the anisotropic characteristics of Reynolds Stress Models (RSM) offer the potential of capturing more of the complex flow phenomena intrinsic of rotating systems. A literature research suggests that this is the first work to assess the EB-RSM (Elliptic Blending RSM), an RSM with low-Reynolds modeling capabilities, on a wind turbine-type rotor under a mildly compressible blade tip flow regime. The results for blade pressure profiles, sectional loads, axial force (thrust) and torque obtained from the steady-state EB-RSM are compared to the reference experimental measurements offered by the New MEXICO campaign, as well as to other CFD data from recent literature. This research includes a Grid Convergence Index (CGI) study and is performed using the commercial multiphysics software Simcenter STAR-CCM+. This work focuses on the unyawed 4.5 m diameter three-bladed MEXICO rotor with -2.3º blade pitch angle rotating at 425.1 rpm under the design free-stream velocity of 15.06 m/s, resulting on a tip speed ratio (TSR) of 6.65, where velocity magnitudes as high as 140 m/s (Mach 0.4) are attained on the suction side of the blade near the tip, with respect to the rotating reference frame, a condition expected to be found in large HAWTs. Grid-converged results obtained on a 6.5 million cell polyhedral mesh delivered pressure loads comparable to the values obtained by other researchers. As an additional output, the authors induce that the loads including skin friction, obtained from continuous integration using mesh resolution, may be considered as a possible reference for the calibration of low-fidelity wind turbine engineering models.*

Keywords: *computational fluid dynamics, aerodynamics, wind energy, turbomachinery, all-Mach coupled flow*

1. INTRODUCTION

Reynolds Stress Models (RSM) are also referred to as Differential Reynolds Stress Models (DRSM) or also Reynolds Stress Transport (RST) Models. This class of Reynolds Averaged Navier-Stokes (RANS) turbulence models differs from the two-equation RANS class on its seven-equation set, six of them responsible for modeling the transport of each one of the six Reynolds stress tensor components individually. Indeed, while RSM models are known to be capable of modeling flows with high anisotropy, two-equation models rely on the so-called Boussinesq assumption (Boussinesq, 1877), or Boussinesq approximation, which is based on the hypothesis of homogeneous and isotropic turbulence fluctuations, where all the six components of the Reynolds stress tensor are the same and linearly proportional to the mean strain rate. Even though such assumption is indeed capable of offering physically sound results for a wide set of applications in some two-equation model implementations, its validity may start to fall apart when flows are characterized by turbulence-induced secondary flows, streamline curvature, swirling flows, transitional flows and flows in rotating systems. This kind of phenomena is easily found in ducted flows and turbomachinery, including horizontal axis wind turbines (HAWTs), where traditional two-equation models should not be employed unless some ad-hoc correction is incorporated (Hellsten and Wallin, 2009). Having that said, it becomes evident the interest of studying the level of accuracy two-equation models are capable to reach in such applications. However, this assessment cannot be properly carried out without adequate references, either from high-quality experimental data or from high-fidelity 3D CFD simulations, such as those offered either by unsteady approaches or by anisotropic steady-state models, which is the case of RSM class. The Elliptic Blending RSM (Manceau and Hanjalić, 2002; Lardeau and Manceau,

2014) here employed was designed to well capture not only the intrinsic anisotropies found on rotating systems, but also the low-Reynolds boundary-layer flows, making it appropriate for modeling flow separation and reattachment, while keeping the so-called SSG formulation of Speziale et al. (1991) in the outer region.

It's in the quest of offering to the wind energy scientific community a high-quality experimental dataset for various flow conditions on a wind turbine-type rotor that an European Union consortium performed the MEXICO (Schepers et al., 2012) and the New MEXICO (Boorsma et al., 2018) measurements, where MEXICO stands for "Model rotor EXperiments In COntrolled conditions". These data have been used by the wind energy CFD scientific community to validate strategies for numerically modeling wind turbines, either using low-fidelity (engineering) methods, such as the Blade Element Momentum (BEM) from Glauert (1935) and the Vortex Wake Models (VWM) from Scully (1967), or high-fidelity methods, where CFD is included. As Zhong et al. (2018) carefully described, while the low-fidelity methods are specially developed for rotary machinery, CFD is a general method that can be used to solve almost all common flow problems on the whole computational domain, in such a way that the rotational effects or tip loss phenomena are naturally modeled, and therefore additional models for capturing such physics are not required as in BEM. Even though CFD comes with a much higher computational cost and the issue of how to choose the appropriate approach to handle turbulence, it is currently being regarded as a high-resolution tool for calibrating low resolution methods (Gómez-Iradi et al., 2010; Campobasso et al., 2016; Herráez, 2016; Bangga, 2018b, 2018a; Rahimi et al., 2018), especially for flow conditions where experimental data is still not available or its acquisition under controlled conditions is impractical (Schreck, 2008; Rahimi et al., 2018), as it is the case of large multi-megawatt HAWTs. Indeed, as of the authors' personal opinion, the real flow phenomena occurring in huge wind turbines is currently much closer to be fully understood by the application of CFD than by experimental campaigns. The current research is therefore a contribution to the quest of the CFD strategies better fitted to correctly capture the complex flow phenomena intrinsic to such applications. These phenomena do include radial flows (Lanzafame et al., 2015; Herráez, 2016; Bangga, 2018b), root and tip flows (Herráez, 2016; Bangga, 2018b; Pirrung and van der Laan, 2018) and the challenge of determining the local angle of attack (Herraéz et al., 2018; Rahimi et al., 2018; Schepers and Schreck, 2019; Wen et al., 2019), as well as the local spanwise flow angle and local drag and lift coefficients as influenced by the aforementioned true flow characteristics. In addition to all these, however, for large HAWTs, the mildly compressible flow phenomena at the blade tip should also be assessed with caution by using CFD strategies capable of capturing it (Carrión et al., 2013), especially if blade tip vortices (Kelly, 2015), aeroelasticity (Farsadi, 2018) and aeroacoustics (Arakawa et al., 2005) are of interest.

To the best of authors' knowledge, the work of O'Brien et al. (2018) on a 0.3 m diameter HAWT model have pioneered the assessment of EB-RSM for wind turbine aerodynamics, and a literature research suggests that the assessment carried out in the present work is the first to consider a mildly compressible flow regime. By coupling the high-fidelity steady-state anisotropy aspects of EB-RSM turbulence model to the reference experimental measurements offered by the New MEXICO campaign, as well as by comparing to other CFD data from recent literature, this work aims to stimulate the development of adequate strategies for the CFD modeling of large HAWTs, as high-fidelity references for the improvement of not only the low-fidelity engineering models, but also of the two-equation CFD turbulence model class.

2. SYSTEMATIC LITERATURE REVIEW

With the objective to review all the literature that had already been published referring to the New MEXICO experiments, a systematic literature review was conducted between 11/25/2019 and 12/30/2019. First, a Google Scholar search was performed using the following search terms: *"New MEXICO" author:boorsma author:schepers*. From the results delivered, 4 materials were selected as including the most relevant information about the desired experimental data, namely (Boorsma and Schepers, 2014b, 2014a, 2016; Boorsma et al., 2018). Then, a search was performed on the works who cited at least one of these selected materials. Documents written in languages different from English, Portuguese, French and Spanish were filtered out. From the remaining collection, 18 documents explicitly reported to have compared the New MEXICO data to full 3D CFD analysis of the rotating rotor, 16 of them in axial (non-yawed) flow conditions. Articles with subscription restrictions that did not report this neither in the title nor in the abstract were filtered out. Among these 16 documents, the comprehensive CFD study reported by Bangga (2018c) was retrieved, which is a compilation of four articles previously published by the same author. Two of these four articles do compare full 3D CFD analysis of the MEXICO rotor in axial flow to the New MEXICO experiments, but they were not delivered by any of the previous Google Scholar searches. This lead to 16 + 2 = 18 research documents comparing the New MEXICO experiments data with full 3D CFD analysis of the rotating rotor in axial flow conditions. Excluding Bangga (2018c), there were thus 17 independent documents from which further insights were drawn out regarding the strategies used for the definition of the computational domain, rotating domain, rotor components, spatial and temporal discretization, flow equations, turbulence model, transition model, inflow turbulence intensity, computational methods, convergence levels and the data extracted from the computations.

Boorsma et al. (2018) was the reference selected in this work for the wind tunnel tests description. The experiments for the uniform axial flow are called by this reference as "Case 1.1", "Case 1.2" and "Case 1.3" respectively for the

inflow speeds of 10.05 m/s, 15.06 m/s and 24.05 m/s. Additionally, all these three reference wind tunnel analysis were performed with blade pitch angle of -2.3º and rotor speed of 425.1 rpm. Among the 17 documents analyzed, only 6 explicitly report to have reproduced the 15.06 m/s design speed case (Case 1.2), chosen for the present turbulence model assessment, delivering clear CFD results for at least one of the three blade load datasets: (1) sectional pressure profiles (2) sectional forces and (3) integral loads. These 6 documents were therefore selected for the "CFD literature" references presented in this work.

3. DESCRIPTION OF THE CASE

The MEXICO rotor is a 4.5 m diameter three-bladed horizontal axis rotor with pre-defined rotating speed. The experimental measurements of Case 1.2 (Boorsma et al., 2018), selected for the purpose of this work, were performed with zig-zag strips on both sides of the blade surface, near the leading edge, until 70% of the rotor radius (Boorsma and Schepers, 2018) to enforce a turbulent boundary layer on them. Because the present study has not the objective to evaluate a transitional model, but a fully turbulent flow modeling instead, it is positive to have such a fully turbulent boundary layer as experimental reference.

As of the computational modeling, the virtual geometry of the MEXICO rotor blade with -2.3º pitch angle was placed inside a 120º periodic computational domain, as depicted in Fig. 1, composed by a 425.1 rpm rotating region (in yellow) with a diameter of 2.2 rotor radius, surrounded by a static region (in grey) with a diameter of 30 rotor radius. The air inlet boundary (dark red) is located 20 rotor radius upstream the blade rotating plane, and the air outlet boundary (brown), 40 rotor radius. The rotating region spans from 2.2 rotor radius upstream to 3.0 rotor radius downstream the blade rotating plane. The rotor tower was not modeled, and the nacelle modelling followed the "semi-infinite" strategy adopted by Lienard and Boisard (2018), reproducing the nacelle geometry (light grey) only upstream the rotor in order to take into account the related velocity increase near the blade root. Downstream the rotor, however, with the objective of removing the influence of nacelle's wake on the overall rotor wake dynamics, a 120º cylindrical wall segment represents the semi-infinite free-slip stream surface with the same radius of the nacelle.

The boundary conditions set in the computational domain shown in Fig. 1 are as follows: dark red is a uniform 15.06 m/s, 294.91 K velocity inlet; brown is a zero-pressure outlet with 294.91 K backflow temperature; dark grey and yellow are periodic interfaces; light grey and the transparent outer grey surfaces are free-slip walls; green is a no-slip wall; and the transparent yellow surface is an internal interface. Turbulence values set on the inlet and for the backflow on the zero-pressure outlet are turbulence intensity (1%) and turbulent viscosity ratio (10.0). The only purpose of the thinner free-slip light grey streamtube (located upstream the semi-infinite nacelle) is to avoid mesh cells shared by both periodic interfaces. All interface cells have a conformal match.

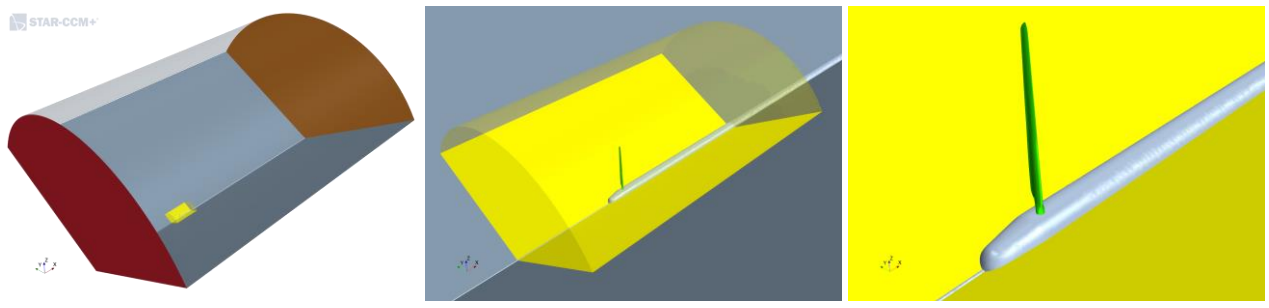

Figure 1. Geometry of the computational domain.

The air flow was modeled by a fully turbulent, compressible, steady-state RANS. Density was modeled as ideal gas, and for dynamic viscosity and thermal conductivity Sutherland's law (Sutherland, 1893) was used. Other air properties were set to constant values: molecular weight to 28.9664 kg/kmol, specific heat to 1003.62 J/kg.K, and turbulent Prandtl number to 0.9. Reference pressure was set to 101,345 Pa (Case 1.2). Calculations were performed in the multiphysics commercial software Simcenter STAR-CCM+ 2020.1.1 Double Precision, with the Roe-FDS (Weiss and Smith, 1995) all-speed preconditioned density-based continuity solver on a coupled solution sequence over four unstructured grid resolutions, the finest mesh totalizing 6.5 million polyhedral cells. Different grid resolutions did not affect the number of near-wall prism layers and their heights, the wall-cell centroid distance from the blade being chosen to keep the wall y+ close to 1.0 and smaller than 2.0, in order to benefit from EB-RSM low-Reynolds turbulence modeling capabilities. STAR-CCM+'s "All y+ Wall Treatment" was employed, as it's designed to give reasonable solutions of the boundary layer flow even if the wall-cell centroid falls within the buffer region of the boundary layer ('Simcenter STAR-CCM+ 2020.1.1 Documentation: Wall Treatment', 2020). STAR-CCM+'s Automatic CFL control was employed; for the finest mesh resolution, it delivered a stable solution for CFL values around 100, and not greater than 1000; but for the coarser meshes, the constant CFL of 100 delivered more stable solutions than using the Automatic CFL control.

4. GRID CONVERGENCE STUDY

Calculations were performed over four grid resolutions with a constant and homogeneous refinement factor of 1.3 (near-wall prism layers excluded), where the axial force on the blade showed an asymptotic behavior for the three most refined meshes. The convergence indexes proposed by Celik et al. (2008) suggest a converged mesh and are presented on Tab. 1, where φ_3, φ_2 and φ_1 are the axial force values obtained from continuous integration using mesh resolution, from root to tip, including skin friction, respectively for the coarse, medium and fine meshes; e_a^{21} is the approximate relative error from the medium to the fine mesh; p is the real convergence order; φ_{ext}^{21} is the asymptotically extrapolated grid-converged axial force; e_{ext}^{21} is the approximate relative error from the fine mesh to the extrapolated value; and GCI_{fine}^{21} is the fine Grid Convergence Index.

Table 1. Grid convergence indexes obtained as proposed by Celik et al. (2008).

$\varphi_3\ [N]$	$\varphi_2\ [N]$	$\varphi_1\ [N]$	e_a^{21}	p	$\varphi_{ext}^{21}\ [N]$	e_{ext}^{21}	GCI_{fine}^{21}
574.1614	563.7252	563.7054	0.00351%	23.89	563.7053	0.00001%	0.00001%

For the finest mesh, which gives the results presented in this paper, all residuals converged below 1.0e-04 on their RMS absolute (non-normalized) values, except for the energy and the turbulence dissipation rate equations. The maximum energy residual is 25 W, but located away from the blade in a cell whose total energy rate is 17,000 W, thus a relative stable oscillation of less than 0.2%. Total energy rate was calculated by multiplying the local specific total energy (J/kg) by the mass flow rate (kg/s) on the mesh cell approximate area, given by $V^{2/3}$, where V is the local cell volume. The maximum turbulence dissipation rate residual is 840 m²/s³ in a cell whose absolute dissipation rate value is 4.0e+07 m²/s³, thus a relative stable oscillation of less than 0.01%. All monitored values of integrals and variables at probe points either stabilized to a constant value or achieved stable oscillations.

5. RESULTS

The chosen flow conditions resulted on velocity magnitudes as high as 140 m/s (Mach 0.4) on the suction side of the blade near the tip, with respect to the rotating reference frame, a condition expected to be found in large HAWTs. A mesh slice at 92% of the rotor radius is seen in Fig. 2 colored by the Mach number. In the same figure, the blade tip with mesh displayed and colored by the y^+ gives an idea of near-wall mesh resolution for well resolving the boundary layer low-Reynolds flow. Finally, the blade tip vortex is made visible by a volume rendering of the Q-Criterion (Dubief and Delcayre, 2000), where the greater the value of Q, the more the magnitude of flow rotation outweighs the magnitude of flow deformation, thus identifying the regions of high angular velocities surrounded by high vorticity, which are characteristic of the vortex cores. The mesh resolution near the blade trailing edge can be visualized in Fig. 3.

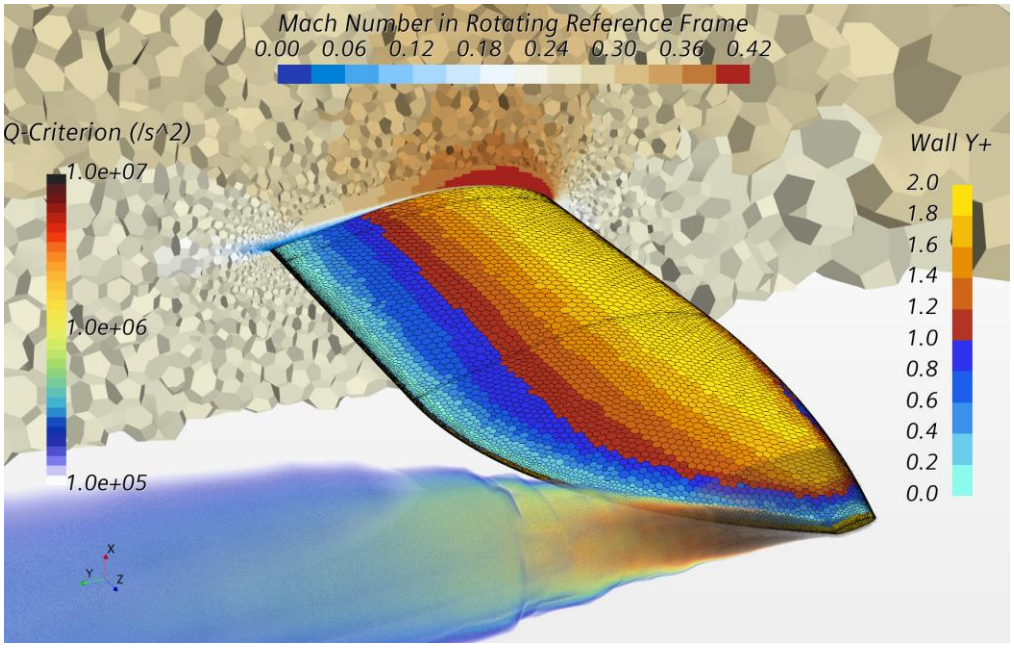

Figure 2. Mesh slice at 92% of the rotor radius colored by the Mach number; blade tip with mesh displayed and colored by the wall y^+; and volume rendering of Q-Criterion to identify the blade tip vortex.

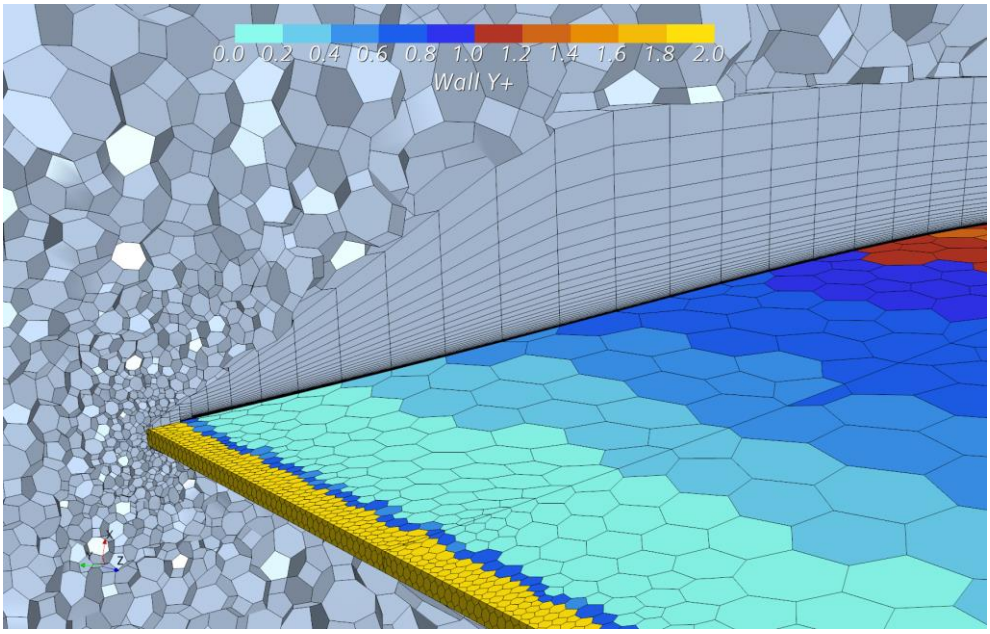

Figure 3. Mesh slice at 92% of the rotor radius near the blade trailing edge. Blade surface colored by wall y^+.

In order to evaluate the ability of EB-RSM to capture the basic flow features, CFD results were compared to the New MEXICO experiments (Boorsma et al., 2018) and to other full 3D CFD data delivered by other researches on the same rotor, air properties and flow conditions. Table 2 provides an overview of the main characteristics of these other computations found in the literature. All the referenced papers have employed steady-state RANS.

Table 2. Overview of the publications containing full 3D CFD calculations of New MEXICO's Case 1.2, whose data was retrieved for comparison.

Publication	**Zhang et al. (2017)**	**Sorensen et al. (2016)**	**Bouhelal et al (2018)**	**Heister (2018)**	**Vimalakan-than and Boorsma (2018)**	**Lienard and Boisard (2018)**
Turbulence models used for comparison	k-kL-ω	k-ω SST	k-ε RNG	Wilcox k-ω; k-ω SST	k-ω SST	k-ω SST
Fully turbulent (FT) or transitional (TR)	TR	TR	TR	Both	FT(1)	Both
Y+ range	N/A	< 2	< 1 - 30	< 1	~ 1(1)	N/A
CFD Code	OpenFOAM	EllipSys3D	ANSYS Fluent 17.2	TAU-Code (DLR)	OpenFOAM and SU2	elsA
Compressible or incompressible	Incompres-sible	Incompres-sible	Incompres-sible	N/A	Incomp. (OF) Comp. (SU2)	N/A
Nacelle modelling	Reproduced	Reproduced	Absent	Absent	Infinite	Semi-infinite
Grid type (structured / unstructured)	Both	N/A	N/A	Both	Unstructured(1)	Structured
Solution sequence (segregated / coupled)	Segregated	N/A	N/A	N/A	Segreg. (OF) (1) Coupl. (SU2) (1)	N/A
Continuity solver (Pressure-based / Density-based)	P-b (SIMPLE)	N/A	N/A	N/A	P-b (OF) (1) D-b (SU2) (1)	N/A

(1) Personal communications.

Pressure profiles are compared in Fig. 4 at five blade sections. Forces per unit length at these same sections are plotted in Fig. 5, both the chord-normal forces and the anti-chordwise (tangential) forces. Finally, Fig. 6 depicts the comparison of integral loads.

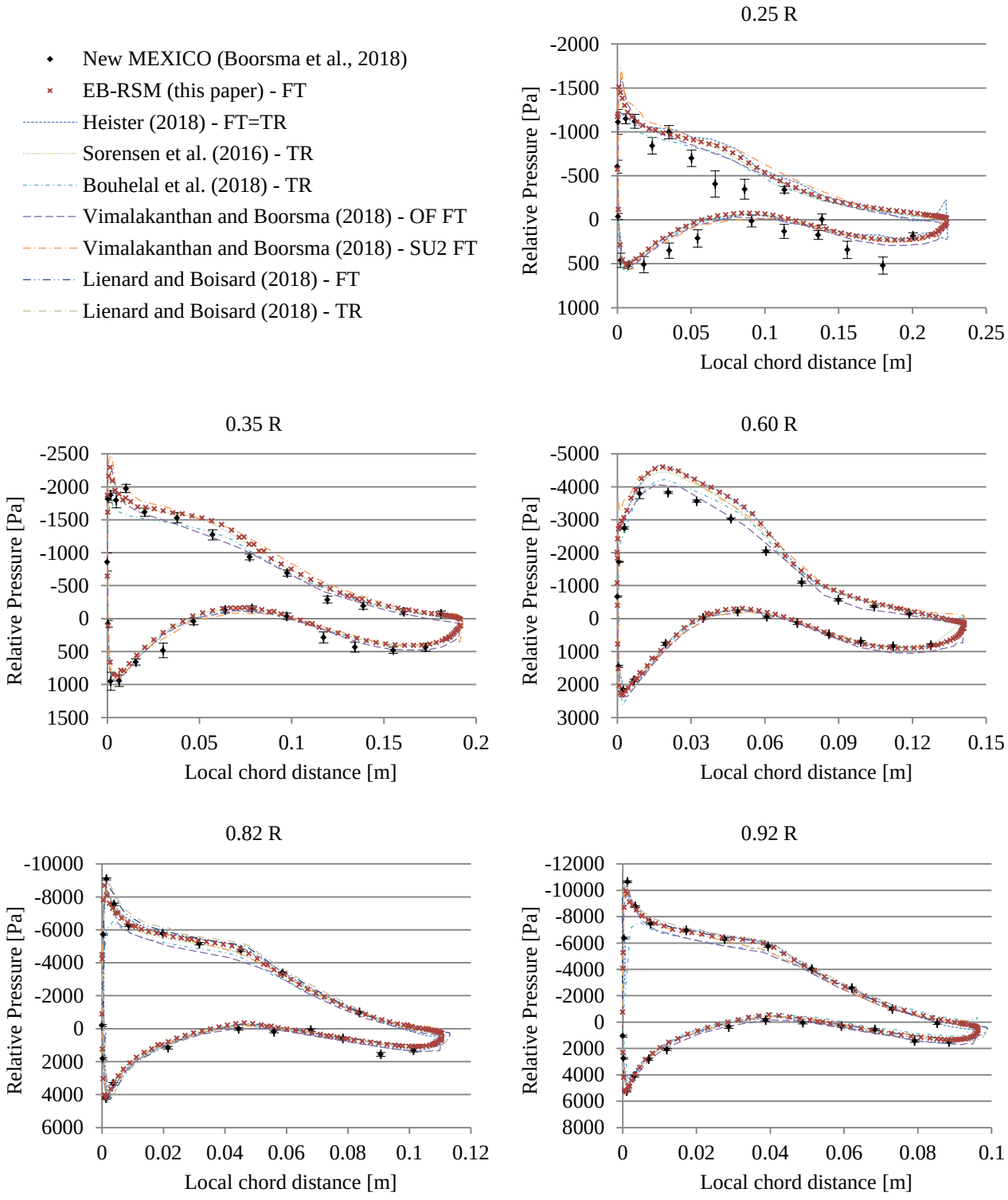

Figure 4. Pressure profiles at the 5 instrumented sections, viz., 25%, 35%, 60%, 82% and 92% of the rotor radius. In the legend, FT stands for "fully turbulent" CFD and TR stands for "transitional" CFD; OF means "OpenFOAM" and SU2 is the name of the other in-house CFD code.

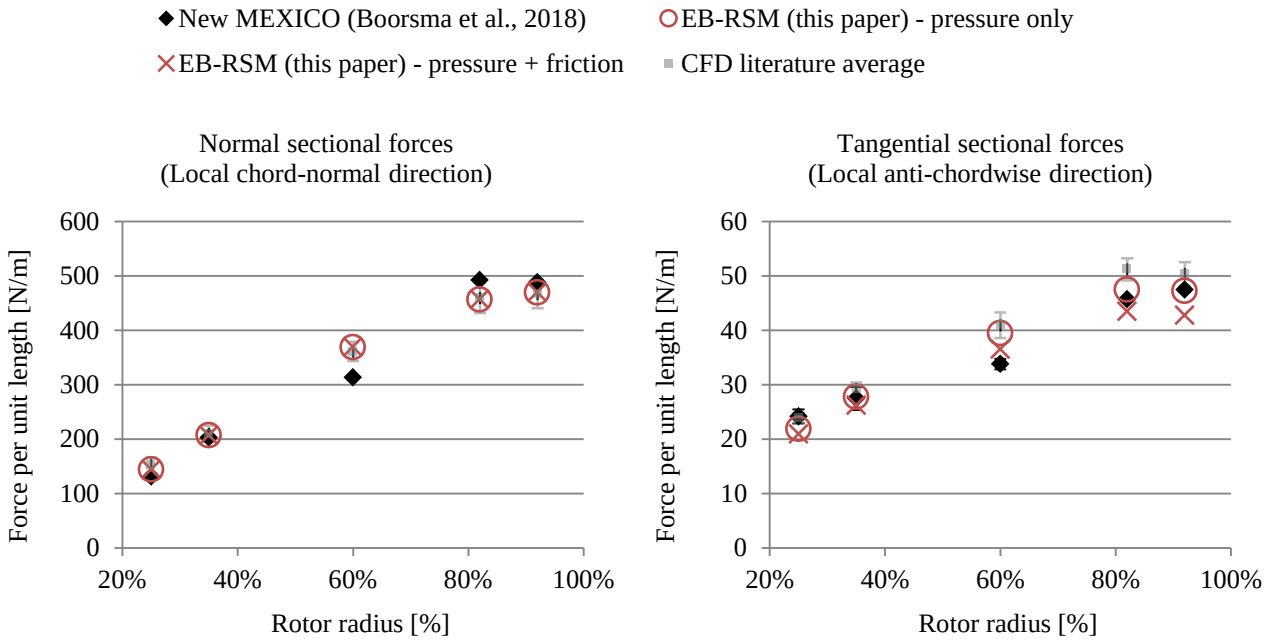

Figure 5. Sectional forces per unit length of a single blade at the 5 instrumented sections, viz., 25%, 35%, 60%, 82% and 92% of the rotor radius. Standard deviation of the analyzed CFD literature is shown by a transparent grey vertical bar. Experimental standard deviations for each blade section are plotted too, yet undistinguishable.

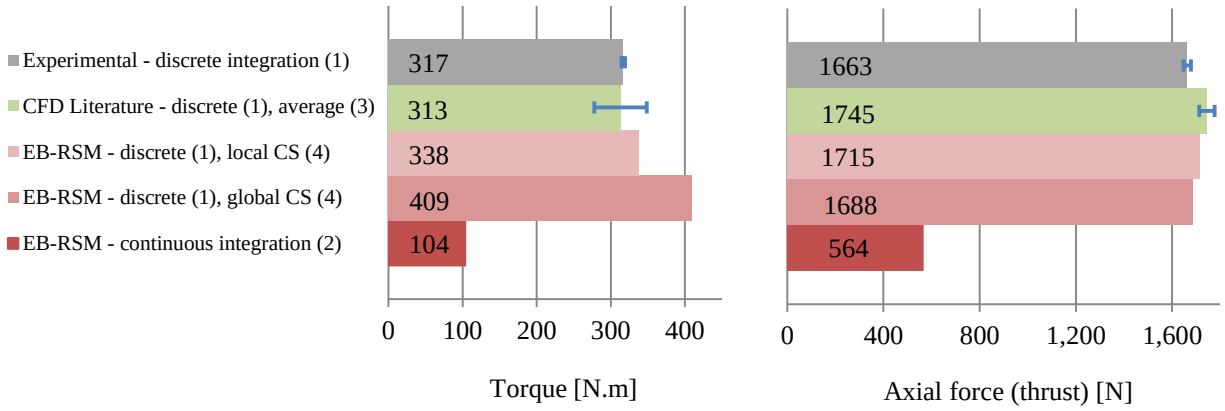

(1) Linear integration from the discrete data of pressure force per unit length at the 5 instrumented sections, assuming (1) zero loads at the blade root and tip and (2) zero skin friction all over the blade, according to the procedure described by (Boorsma et al., 2018).

(2) Integration from the continuous CFD pressure data using mesh resolution, from root to tip, including skin friction, using global CS[4].

(3) (Sørensen et al., 2016; Zhang et al., 2017; Bouhelal et al., 2018; Heister, 2018; Lienard and Boisard, 2018; Vimalakanthan and Boorsma, 2018). Information regarding the usage of global or local CS[4] could not be retrieved from these sources.

(4) Global CS (coordinate system): for the axial force, integrated data points to the global +X axis (rotor axial direction); for the torque, it points to the global –Y axis (blade movement direction on the rotating plane). Local CS: for the axial force, integrated data points to the local chord-normal direction; for the torque, it points to the local anti-chordwise direction.

Figure 6. Integral loads on a single blade, with standard deviation bars plotted in blue.

The contribution of friction force to reduce the net tangential force is observable in Fig. 5, being more pronounced towards the blade tip because of the greater velocities relative to the rotating reference frame.

Figure 6, beyond the integral pressure loads obtained according to the procedure described by Boorsma et al. (2018), it also provides the load values produced by this research including skin friction, obtained from continuous

integration using mesh resolution. Even though the delivered values (104 N.m for blade torque and 564 N for blade thrust) are significantly different from the loads obtained using the aforementioned methodology, the latter is numerically more precise than the linear integration of discrete values, and might be closer to the physical reality of New MEXICO's Case 1.2.

6. CONCLUSIONS

This research have demonstrated the ability of EB-RSM to deliver blade pressure loads comparable to the New MEXICO experiments of Case 1.2 and to other CFD studies on the same case. Still, among the articles whose data was extracted for comparison, no information was found on loads including skin friction. Thus, considering that the present study (1) solved a compressible flow to address the Mach numbers greater than 0.4 near the blade tip, (2) used a turbulence model that is tailored for the intrinsic anisotropy features and for the low-Reynolds boundary layer flow and (3) is mesh-converged according to the GCI study, the authors induce that the presented loads including skin friction obtained from continuous integration using mesh resolution may be considered closer to the physical reality of New MEXICO's Case 1.2, and thus a possible reference for the calibration of low-fidelity wind turbine engineering models.

7. ACKNOWLEDGEMENTS

The experimental data used have been supplied by the consortium which carried out the EU FP5 project MEXICO: 'Model rotor EXperiments In COntrolled conditions'. The consortium received additional support to perform the New MEXICO measurements from the EU projects ESWIRP and INNWIND.EU. The authors express deep gratitude to the consortium for sharing their experimental data, to whom the research outputs delivered in this work the authors also dedicate.

The authors are also thankful to Siemens Digital Industries Software, *Centro Nacional de Supercomputação* (CESUP), UFRGS's School of Engineering Library and to *Conselho Nacional de Desenvolvimento Científico e Tecnológico* (CNPq).

Last but not least, our deep gratitude to the researchers who generously provided us further details on the works they performed, namely Mr. Galih Bangga, Mr. Kisorthman Vimalakanthan, Mr. Koen Boorsma, Mr. Wei Zhong, Mr. Iván Herráez and Mr. Keita Kimura.

Dataset for the blade loads computed using EB-RSM can be obtained from https://doi.org/10.5281/zenodo.4107206 under a Creative Commons Attribution license.

8. REFERENCES

Arakawa, C. *et al.* (2005) 'Numerical Approach for Noise Reduction of Wind Turbine Blade Tip with Earth Simulator', *Journal of the Earth Simulator*, 2(March), pp. 11–33.

Bangga, G. (2018a) 'Comparison of blade element method and CFD simulations of a 10 MW wind turbine', *Fluids*. Multidisciplinary Digital Publishing Institute, 3(4), p. 73. doi: 10.3390/fluids3040073.

Bangga, G. (2018b) *Three-dimensional flow in the root region of wind turbine rotors*. Kassel University Press. doi: 10.19211/KUP9783737605373.

Bangga, G. (2018c) *Three-dimensional flow in the root region of wind turbine rotors*.

Boorsma, K. *et al.* (2018) *Final report of IEA wind task 29 Mexnext (Phase 3), Wind Energy*. ECN Wind Energy.

Boorsma, K. and Schepers, J. G. (2014a) 'Mexnext-II - The Latest Results on Experimental Wind Turbine Aerodynamics'.

Boorsma, K. and Schepers, J. G. (2014b) *New MEXICO experiment: Preliminary overview with initial validation*.

Boorsma, K. and Schepers, J. G. (2016) 'Rotor experiments in controlled conditions continued: New Mexico', in *Journal of Physics: Conference Series*. Institute of Physics Publishing. doi: 10.1088/1742-6596/753/2/022004.

Boorsma, K. and Schepers, J. G. (2018) *Description of Experimental Setup: New MEXICO Experiment (ECN-X--15-093_v3)*.

Bouhelal, A. *et al.* (2018) 'Numerical investigation of turbulent flow around a recent horizontal axis wind Turbine using low and high Reynolds models', *Journal of Applied Fluid Mechanics*, (11), pp. 151–164.

Boussinesq (1877) 'Essai sur la théorie des eaux courantes', *Impr. nationale*.

Campobasso, M. S., Drofelnik, J. and Gigante, F. (2016) 'Comparative assessment of the harmonic balance Navier–Stokes technology for horizontal and vertical axis wind turbine aerodynamics', *Computers and Fluids*. Elsevier Ltd, 136, pp. 354–370. doi: 10.1016/j.compfluid.2016.06.023.

Carrión, M. *et al.* (2013) 'Implementation of all-Mach Roe-type schemes in fully implicit CFD solvers - demonstration for wind turbine flows', *International Journal for Numerical Methods in Fluids*, 73(8), pp. 693–728. doi: 10.1002/fld.3818.

Celik, I. B. *et al.* (2008) 'Procedure for estimation and reporting of uncertainty due to discretization in CFD applications', *Journal of Fluids Engineering, Transactions of the ASME*, 130(7), pp. 0780011–0780014. doi: 10.1115/1.2960953.

Dubief, Y. and Delcayre, F. (2000) 'On coherent-vortex identification in turbulence', *Journal of Turbulence*, 1. doi: 10.1088/1468-5248/1/1/011.

Farsadi, T. (2018) *Aeroelastic Analysis of Composite Wings and Wind Turbine Blades Including Geometrical Nonlinearity and Compressibility*. Middle East Technical University.

Glauert, H. (1935) 'Airplane Propellers', in Durand, W. F. (ed.) *Aerodynamic Theory*. Berlin, Heidelberg: Springer Berlin Heidelberg, pp. 169–360. doi: 10.1007/978-3-642-91487-4_3.

Gómez-Iradi, S., Barakos, G. N. and Munduate, X. (2010) 'A CFD investigation of the near-blade 3D flow for a complete wind turbine configuration', *European Wind Energy Conference and Exhibition 2010, EWEC 2010*, 3, pp. 2212–2240.

Heister, C. C. (2018) 'RANS simulation of the new Mexico rotor experiment including laminar-turbulent transition', in *Notes on Numerical Fluid Mechanics and Multidisciplinary Design*. Springer Verlag, pp. 729–739. doi: 10.1007/978-3-319-64519-3_65.

Hellsten, A. and Wallin, S. (2009) 'Explicit algebraic Reynolds stress and non-linear eddy-viscosity models', *International Journal of Computational Fluid Dynamics*. Taylor & Francis, 23(4), pp. 349–361. doi: 10.1080/10618560902776828.

Herráez, I. (2016) 'Numerical Analysis of Wind Turbine Aerodynamics', p. 130.

Herraéz, I., Daniele, E. and Gerard Schepers, J. (2018) 'Extraction of the wake induction and angle of attack on rotating wind turbine blades from PIV and CFD results', *Wind Energy Science*. Copernicus GmbH, 3(1), pp. 1–9. doi: 10.5194/wes-3-1-2018.

Kelly, R. T. (2015) *Numerical prediction of the spatial and temporal characteristics of the aero-optical disturbance produced by a helicopter in hover*. University of Notre Dame.

Lanzafame, R., Mauro, S. and Messina, M. (2015) 'Evaluation of the radial flow effects on micro HAWTs through the use of a transition CFD 3D model - Part I: State of the art and Numerical model review', in *Energy Procedia*. Elsevier Ltd, pp. 156–163. doi: 10.1016/j.egypro.2015.12.011.

Lardeau, S. and Manceau, R. (2014) 'Computations of complex flow configurations using a modified Elliptic-Blending Reynolds-Stress model', in *Proc. 10th ERCOFTAC Int. Symp. on Eng. Turb. Modelling and Measurements*.

Lienard, C. and Boisard, R. (2018) 'Investigation of the MEXICO rotor aerodynamics in axial flow, including boundary layer transition effects', in *Wind Energy Symposium, 2018*. American Institute of Aeronautics and Astronautics Inc, AIAA. doi: 10.2514/6.2018-1495.

Manceau, R. and Hanjalić, K. (2002) 'Elliptic blending model: A new near-wall Reynolds-stress turbulence closure', *Physics of Fluids*, 14(2), pp. 744–754. doi: 10.1063/1.1432693.

O'Brien, J. M. *et al.* (2018) 'An assessment of commercial CFD turbulence models for near wake HAWT modelling', *Journal of Wind Engineering and Industrial Aerodynamics*. Elsevier B.V., 176, pp. 32–53. doi: 10.1016/j.jweia.2018.03.001.

Pirrung, G. R. and van der Laan, M. P. (2018) 'A simple improvement of a tip loss model for actuator disc and actuator line simulations', *Wind Energy Science Discussions*, pp. 1–13. doi: 10.5194/wes-2018-59.

Rahimi, H. *et al.* (2018) 'Evaluation of different methods for determining the angle of attack on wind turbine blades with CFD results under axial inflow conditions', *Renewable Energy*. Elsevier Ltd, 125, pp. 866–876. doi: 10.1016/j.renene.2018.03.018.

Schepers, J. G. *et al.* (2012) *Final report of IEA Task 29, Mexnext (Phase 1): Analysis of Mexico wind tunnel measurements*.

Schepers, J. G. and Schreck, S. J. (2019) 'Aerodynamic measurements on wind turbines', *Wiley Interdisciplinary Reviews: Energy and Environment*. John Wiley and Sons Ltd. doi: 10.1002/wene.320.

Schreck, S. (2008) *IEA Wind Annex XX: HAWT Aerodynamics and Models from Wind Tunnel Measurements*.

Scully, M. P. (1967) *A Method of Computing Helicopter Vortex Wake Distortion*.

'Simcenter STAR-CCM+ 2020.1.1 Documentation: Wall Treatment' (2020). Siemens Digital Industries Software.

Sørensen, N. N. *et al.* (2016) 'CFD computations of the second round of MEXICO rotor measurements', in *Journal of Physics: Conference Series*. Institute of Physics Publishing. doi: 10.1088/1742-6596/753/2/022054.

Speziale, C. G., Sarkar, S. and Gatski, T. B. (1991) 'Modelling the pressure-strain correlation of turbulence : An invariant dynamical systems approach', *Journal of Fluid Mechanics*. 2006/04/26. Cambridge University Press, 227, pp. 245–272. doi: 10.1017/S0022112091000101.

Sutherland, W. (1893) ' LII. The viscosity of gases and molecular force ', *The London, Edinburgh, and Dublin Philosophical Magazine and Journal of Science*, 36(223), pp. 507–531. doi: 10.1080/14786449308620508.

Vimalakanthan, K. and Boorsma, K. (2018) *Baseline Mexico rotor CFD simulations with SU2 and OpenFOAM*.

Weiss, J. M. and Smith, W. A. (1995) 'Preconditioning applied to variable and constant density flows', *AIAA Journal*, 33(11), pp. 2050–2057. doi: 10.2514/3.12946.

Wen, B. *et al.* (2019) 'A numerical study on the angle of attack to the blade of a horizontal-axis offshore floating wind turbine under static and dynamic yawed conditions', *Energy*. Elsevier Ltd, 168, pp. 1138–1156. doi: 10.1016/j.energy.2018.11.082.

Zhang, Y., van Zuijlen, A. and van Bussel, G. (2017) 'The MEXICO rotor aerodynamic loads prediction: ZigZag tape effects and laminar-turbulent transition modeling in CFD', *Journal of Wind Engineering and Industrial Aerodynamics*. Elsevier B.V., 168, pp. 152–163. doi: 10.1016/j.jweia.2017.06.002.

Zhong, W. *et al.* (2018) 'Accurate RANS simulation of wind turbine stall by turbulence coefficient calibration', *Applied Sciences (Switzerland)*. Multidisciplinary Digital Publishing Institute, 8(9), p. 1444. doi: 10.3390/app8091444.

9. RESPONSIBILITY NOTICE

The authors are the only responsible for the printed material included in this paper.